



## An effective retinal blood vessel segmentation method using multi-scale line detection

Uyen T.V. Nguyen<sup>a,\*</sup>, Alauddin Bhuiyan<sup>a</sup>, Laurence A.F. Park<sup>b</sup>, Kotagiri Ramamohanarao<sup>a</sup>

<sup>a</sup> Department of Computer Science and Software Engineering, The University of Melbourne, Victoria, Australia

<sup>b</sup> School of Computing, Engineering and Mathematics, The University of Western Sydney, New South Wales, Australia

### ARTICLE INFO

#### Article history:

Received 13 April 2012

Received in revised form

27 June 2012

Accepted 9 August 2012

Available online 21 August 2012

#### Keywords:

Retinal image

Vessel extraction

Line detector

Central reflex

### ABSTRACT

Changes in retinal blood vessel features are precursors of serious diseases such as cardiovascular disease and stroke. Therefore, analysis of retinal vascular features can assist in detecting these changes and allow the patient to take action while the disease is still in its early stages. Automation of this process would help to reduce the cost associated with trained graders and remove the issue of inconsistency introduced by manual grading. Among different retinal analysis tasks, retinal blood vessel extraction plays an extremely important role as it is the first essential step before any measurement can be made. In this paper, we present an effective method for automatically extracting blood vessels from colour retinal images. The proposed method is based on the fact that by changing the length of a basic line detector, line detectors at varying scales are achieved. To maintain the strength and eliminate the drawbacks of each individual line detector, the line responses at varying scales are linearly combined to produce the final segmentation for each retinal image. The performance of the proposed method was evaluated both quantitatively and qualitatively on three publicly available DRIVE, STARE, and REVIEW datasets. On DRIVE and STARE datasets, the proposed method achieves high local accuracy (a measure to assess the accuracy at regions around the vessels) while retaining comparable accuracy compared to other existing methods. Visual inspection on the segmentation results shows that the proposed method produces accurate segmentation on central reflex vessels while keeping close vessels well separated. On REVIEW dataset, the vessel width measurements obtained using the segmentations produced by the proposed method are highly accurate and close to the measurements provided by the experts. This has demonstrated the high segmentation accuracy of the proposed method and its applicability for automatic vascular calibre measurement. Other advantages of the proposed method include its efficiency with fast segmentation time, its simplicity and scalability to deal with high resolution retinal images.

© 2012 Elsevier Ltd. All rights reserved.

### 1. Introduction

Changes in retinal vascular structures are manifestations of many systemic diseases such as diabetes, hypertension, cardiovascular disease and stroke. For example, changes in vessel calibre, branching angle or vessel tortuosity are results of hypertension [1,2]. The onset of neovascularization is a sign of diabetic retinopathy [3], a complication of diabetes which is the leading cause of blindness in developed countries. The presence of arteriovenous nicking is an important precursor of stroke [4,5]. The early detection of these changes is extremely important in order to perform early intervention and prevent the patients from major vision loss. To quantify these features for medical diagnosis, accurate vessel segmentation plays a critical role. Although many methods have been proposed, significant

improvement is still a necessity due to the limitations in state-of-the-art methods, which include:

- poor segmentation in the presence of vessel central light reflex (i.e., bright strip along the centre of a vessel).
- poor segmentation at bifurcation and crossover regions.
- the merging of close vessels.
- the missing of small vessels.
- false vessel detection at the optic disk and pathological regions.

Among the problems mentioned above, the first three are most important due to their great impact on the quality of the vascular network obtained. For example:

- if central reflex pixels are not recognized as part of a vessel, the vessel may be misunderstood as two vessels.
- if two close vessels are merged together, they will be considered as one wide vessel.

\* Corresponding author. Tel.: +61 4 3168 1063; fax: +61 3 9349 4596.

E-mail address: [thivun@student.unimelb.edu.au](mailto:thivun@student.unimelb.edu.au) (U.T.V. Nguyen).

- poor segmentation such as the disconnection at vessel crossover regions (where two vessels cross each other) will cause difficulties for the vessel tracking process.

These will lead to the inaccuracy in vascular network analysis such as the identification of individual vessel segments, vessel calibre measurement, or vascular abnormality (i.e., arteriovenous nicking) detection.

The segmentation results of some existing methods on a cropped retinal image with the presence of central reflex, close vessels and crossover points are shown in Fig. 1 to demonstrate the limitations of current approaches. Vessel disconnection is found in Staal et al. [6] result, while vessel merging is present in Soares et al. [7] result. Missing of central part of vessels due to vessel central reflex are found in both Staal and Soares et al. results. The problem with the segmentation produced by Ricci-line [8] method is the partial merging of two close vessels and the spurious segmentation at the crossover point. Even though the Ricci-svm [8] method produces accurate segmentation at these regions, it fails to detect small vessels.

The contribution of this paper is a novel segmentation method that is effective in dealing with the problems mentioned above. The underlying technique of the proposed method is a linear combination of line detectors at different scales to produce the vessel segmentation for each retinal image. A basic line detector uses a set of approximated rotated straight lines to detect the vessels at different angles. The difference between the average gray level of the winning line (the line with maximum average gray level) and the average gray level of the surrounding window provides a measure of 'vesselness' of each image pixel. The proposed method is based on an observation that by changing the length of the aligned lines, line detectors at different scales are achieved. Long length line detectors have shown to be effective in dealing with central reflex. However, we show later in this article that they tend to merge close

vessels and produce false positives along the vessels. Short length line detectors have shown improvements of these situations but they introduce background noise in the image. In order to maintain the strength and eliminate the drawback of each individual line detector, line responses at different scales are linearly combined to produce the segmentation for each retinal image. Experimental results have shown that the proposed method is an attractive method for retinal vessel segmentation since:

- it gives high segmentation accuracy especially at regions around the vessels. This is reflected by the high local accuracy and the ability of the proposed method to provide accurate vessel width measurement.
- it is an unsupervised method which does not require the manual segmentation of vessels for training and the performance does not depend on the training set.
- it is efficient with fast segmentation time.
- it can be easily extended to perform on high resolution retinal images.

The segmentation result of the proposed method, which is shown in Fig. 1(f), has demonstrated the strengths mentioned above.

The rest of this paper is organized as follows. Section 2 provides an overview of state-of-the-art vessel segmentation methods. Details of the proposed method are described in Section 3. Section 4 presents the experimental results obtained on DRIVE and STARE datasets while the performance on REVIEW dataset is presented in Section 5. Finally, we conclude the paper with Section 6.

## 2. Related works

In response to the importance of the vessel segmentation problem, a large number of methods have been introduced in the literature.

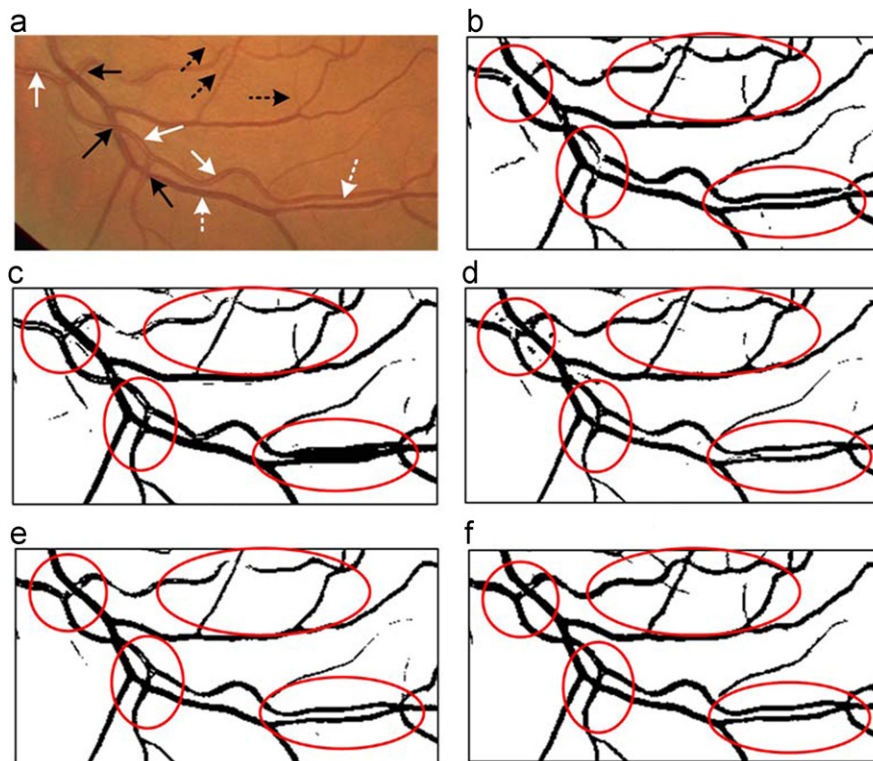


**Fig. 1.** Illustration of the limitations of existing methods: (a) a cropped retinal image shows the presence of vessel central light reflex (white solid arrows), close vessels (white dashed arrows), artery-vein crossing (black solid arrows), and small vessels (black dashed arrows) and segmentations obtained by (b) Staal et al. method [6]; (c) Soares et al. method [7]; (d) Ricci-line method [8]; (e) Ricci-svm method [8]; and (f) the proposed method. The segmentation result of the proposed method has demonstrated its effectiveness when providing accurate segmentation at the specified regions while being able to detect those small vessels.

A complete review of existing methods for retinal blood vessel segmentation can be referenced at [9]. For completeness, we briefly summarize state-of-the-art methods in this section.

The first proposed methods [10–15] are based on tracking techniques to trace the vessels starting from some seed points (which are identified either manually or automatically) and following the vessel center line guided by local information. An advantage of tracking based methods is its efficiency since only pixels close to the initial positions are examined and evaluated. In addition, important information (i.e., vessel diameter and branching points) are often extracted together with the vascular network. However, a drawback of these methods is that sophisticated methods have to be used to deal with a bifurcation or crossover point due to the complexity of the intensity profile at these regions. Since vessel branching or crossover points are not well modeled, this approach often tends to terminate at these points and this leads to the incompleteness in the detection result.

Another approach is the use of matched filter concept [16] for blood vessel enhancement. This approach is based on the assumption that the intensity profile along the cross-section of a vessel has the shape of a Gaussian. A set of 12 Gaussian shaped filters is used to match the vessel at different directions. For each pixel, the maximum response is retained. Different variants [17–20] have been proposed to improve the performance of the original matched filter response, ranging from the use of a threshold probing technique [17], ‘double-sided’ thresholding [19], or the first order derivative of Gaussian image [20] to provide a better thresholding method and reduce false vessel responses at non-vessel structures. A limitation of matched filter based methods is its naive assumption that the cross-sectional intensity profile of a vessel follows the shape of a Gaussian, which is not always the case (for example, in the presence of central reflex). Moreover, the assumptions that the vessels are piece-wise linear and have constant width along a certain distance make it difficult to adapt to the variations in vessel width and orientations.

Recently, there is an emerging trend of using supervised methods [6–8,21–26] to perform this segmentation problem. Methods belonging to this category often follow the same framework where each image pixel is represented by a feature vector, which is computed using local or global information of the image. A supervised classifier (ranging from the use of artificial neural networks [21], kNN [6,22], support vector machines [8,26], Bayesian classifier [7], etc.) is used to train the model and classify each image pixel as vessel or background. Supervised methods have been shown to provide higher accuracy than other unsupervised methods. However, they require the ground truth segmentations for training the models which is not always available in real life applications. Furthermore, these methods often require the ‘re-training’ process when performing on the new set of images to achieve optimal performance. In other words, the performance of these methods is highly dependent on the training dataset.

Besides the three main approaches mentioned above, a number of alternative methods have been proposed. The method proposed by Zana et al. [27] is based on the fact that vessels are piecewise linear and connected. Hence, mathematical morphological operators with linear structuring elements are used to enhance and differentiate the vessels from the background. Jiang et al. [28] propose a multi-threshold probing technique to threshold the image at different levels and uses a verification procedure to detect the vessels in the segmented images. The final segmentation is obtained by a combination of those segmented images returned in each step. Vermeer et al. [29] use the Laplacian filter and thresholding to enhance and extract blood vessels from retinal images. A method based on morphological closing operator is then applied to fill in vessel central light reflex. In [30], the local maxima over scales of the gradient magnitude and the maximum principle

curvature are used as two features to classify each pixel as vessel or background using multiple pass region growing process. Lam et al. [31] use the gradient vector field to detect vessel like objects while employing the normalized gradient vector field to detect the vessel centerlines. A pruning step to remove all vessel pixels that are far away from the centerlines is employed to reduce falsely detected vessels. Lam et al. [32] propose a method to deal with both bright and dark lesions in an abnormal retina. Three different concavity measures are proposed to detect the vessels and distinguish the vessels from the bright and dark lesions. Vlachos et al. [33] employ a multi-scale line-tracking procedure to trace the vessels starting from a set of seed pixels (determined by the brightness selection rule) and terminate when the cross-sectional profile is invalid. The image maps at different scales are then combined together to produce a multi-scale image map.

### 3. Proposed segmentation method

In this section, we first review the basic line detector (which was first used as a means for vessel-background classification by Ricci et al. [8]) upon which our method is built. We then present the proposed generalized line detector and the method to combine the line detectors at varying scales to produce the final segmentation for a retinal image.

#### 3.1. Basic line detector

The basic line detector works on the inverted green channel of a retinal image where the vessels appear brighter than the background. At each pixel position, a window of size  $W \times W$  pixels is identified and the average gray level is computed as  $I_{avg}^W$ . Twelve lines of length  $W$  pixels oriented at 12 different directions (angular resolution of  $15^\circ$ ) passing through the centered pixels are identified and the average of gray levels of pixels along each line is computed. The line with the maximum value is called the ‘winning line’ and its value is defined as  $I_{max}^W$ . The line response at a pixel is then computed as:

$$R_W = I_{max}^W - I_{avg}^W \quad (1)$$

The underlying idea behind this is that if the considered pixel is a vessel pixel, the response obtained will be large due to the alignment of the winning line along the vessel. In contrast, the response is low for a background pixel due to the small difference between the average gray level of the winning line and the surrounding window. The basic line detector has one parameter to be set, the window size  $W$ , which is chosen to ensure that the window of the pixel at the center of the vessel consists of an approximately equal number of vessel and background pixels. Thus, it is often set as twice of the typical vessel width in an image set. For example, it has been shown that  $W=15$  is a good choice for retinal images in DRIVE dataset [6] where the typical vessel width is 7–8 pixels [8].

The basic line detector has shown to be effective when dealing with the vessel central light reflex. In the presence of central reflex, the intensity values of pixels in the middle of a vessel become lower than its surrounding pixels instead of achieving maximum values as in a normal vessel. This often leads to the misclassification of these pixels as background due to the proximity in their intensity values. However, the line detector can recognize them as part of the vessel due to the fact that the winning line includes only a small number of ‘central reflex’ pixels. As a result, its average value is not affected much by these pixels which results in large responses like those of vessel pixels. Also, thanks to the use of long length lines that span through the whole surrounding window, most of background pixels are

correctly classified and the response image is almost free of background noise. The response image produced by the basic line detector on a retinal image is presented in Fig. 2(a).

However, the three drawbacks of the basic line detector include: (1) it tends to merge close vessels; (2) it produces an extension at crossover points; (3) it produces false vessel responses at background pixels near strong vessels (vessels with high intensity values in images where vessels appear brighter than the background). These can be observed in the three segmentation patches as shown in Fig. 2(b). The false vessel responses along a strong vessel can be seen in the top segmentation while the extension at two crossover points can be observed in the middle one. The partial merging of two close vessels is presented in the bottom image. In these cases, the aligned line gets high average value due to the inclusion of pixels of surrounding vessels, which leads to an unexpected large response value which is similar to those of vessel pixels. These situations are depicted in Fig. 3.

### 3.2. Multi-scale line detectors

To overcome the three drawbacks mentioned above, we propose to generalize the basic line detector by varying the length

of the aligned lines. The generalized line detector is defined as:

$$R_W^L = I_{max}^L - I_{avg}^W \quad (2)$$

where  $1 \leq L \leq W$ ,  $I_{max}^L$  and  $I_{avg}^W$  are defined as above. By changing the values of  $L$ , line detectors at different scales are achieved. Fig. 4 depicts a line detector with  $W=15$  and  $L=9$  where 12 lines of 9 pixel length are placed on top of a window of  $15 \times 15$  pixels.

The main idea behind this is that line detectors with shorter lengths will avoid the inclusion of surrounding vessel pixels and hence, give correct responses to three situations presented in Fig. 3. To demonstrate this improvement, the responses of the basic line detector ( $R_{15}$ ) and generalized line detector ( $R_{15}^3$ ) at different pixel positions (Fig. 5) are examined and presented in Table 1. It can be seen that the basic line detector returns high responses to background pixels for three cases (d)–(f) while the generalized line detector gives much lower values for these cases, which makes it possible to distinguish vessel and background pixels for all mentioned cases.

The response image produced by the generalized line detector ( $W=15, L=3$ ) on the same image of Fig. 2(a) is presented in Fig. 6(a). The three segmentation patches presented in Fig. 6(b) have demonstrated the improvements of the generalized line detector: there is no false vessel responses along the strong vessel (top image), segmentation at two crossover points are more accurate

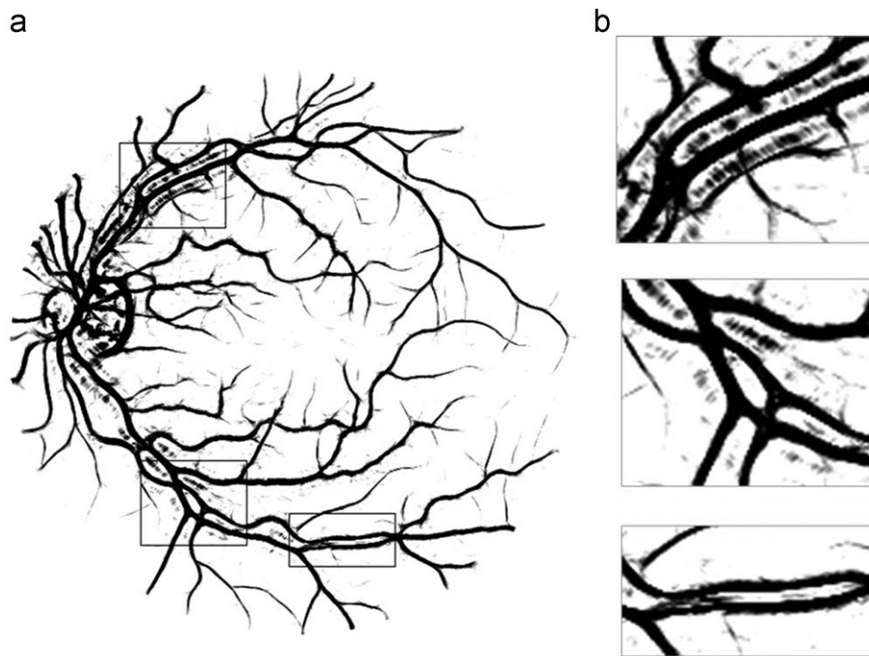


**Fig. 2.** (a) Line strength image of the basic line detector ( $W=15$ ) on a retinal image and (b) its segmentation results at some selective image patches showing the false vessel responses at: background pixels close to strong vessels (first row), at crossover points (second row), and at background pixels between two close vessels (last row). (The vessels are shown in black in this figure for better visualization.)

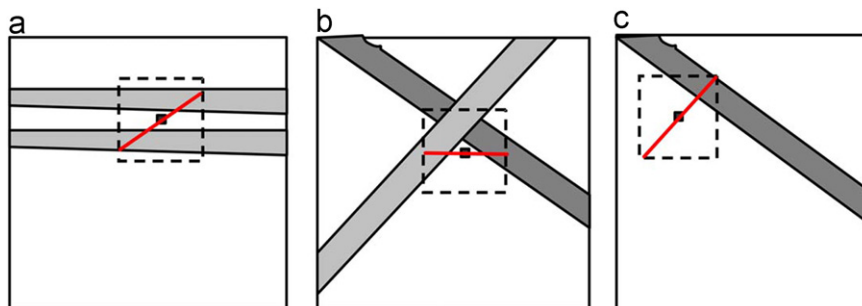


**Fig. 3.** Three situations where the basic line detector gives false responses: (a) at a background pixel between two close vessels; (b) at a background pixel at the corner of a crossover point; (c) at a background pixel near a strong vessel.

(middle image), and two close vessels are well separated (bottom image). However, it can be seen that background noise is introduced in the whole image as a result of reducing the line length. To overcome this problem, line responses at varying scales are linearly combined as described in the next section.

We should note that the raw response values returned by the line detector at each scale are in a narrow range, which results in a very low contrast between the vessels and the background. For example, the raw response image of generalized line detector ( $W = 15, L = 3$ ) (Fig. 7(a)) on a retinal image has shown that the vessels and background are in very low contrast since the intensity range is from  $-0.1709$  to  $0.2764$  with a mean and standard deviation values of  $0.0046$  and  $0.0231$ , respectively. To enhance the contrast in these images, we standardize the values of the raw response image to make it have zero mean and unit standard deviation distribution:

$$R' = \frac{R - R_{mean}}{R_{std}} \quad (3)$$

where  $R'$  is the standardized response value,  $R$  is the raw response value,  $R_{mean}$  and  $R_{std}$  are the mean and standard deviation of the raw response values, respectively. The main purpose of this standardization is to keep the distribution of the intensity values unchanged (hence, retaining the differentiation between the vessels and the background in the standardized image) but spread out the intensity values to a wider range to achieve a better contrast between the vessels and the background. The corresponding standardized image is

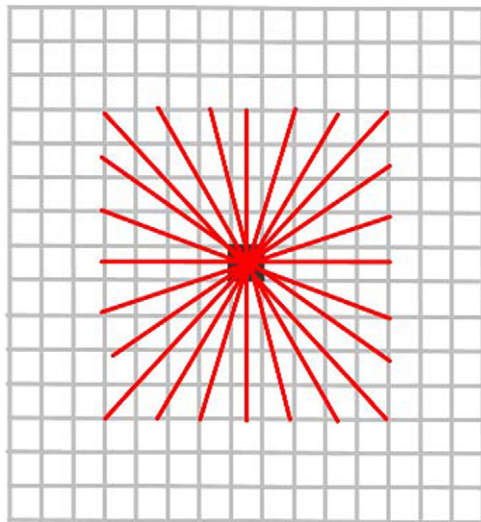


Fig. 4. A generalized line detector with  $W = 15$  and  $L = 9$ .

presented in Fig. 7(b). Clearly, the standardization has significantly improved the vessel and background contrast. This normalization was applied to the response images produced by line detectors at different scales before applying to the combination process.

### 3.3. Combination method

In the combination process, we assign the same weight for each scale and the final segmentation is the linear combination of line responses of different scales. The response at each image pixel is defined as:

$$R_{combined} = \frac{1}{n_L + 1} \left( \sum_L R_W^L + I_{igc} \right) \quad (4)$$

where  $n_L$  is the number of scales used,  $R_W^L$  is the response of line detector at scale  $L$ , and  $I_{igc}$  is the value of the inverted green channel at the corresponding pixel. The original green channel is included into the combination since it provides additional information to discriminate the proximity between the blood vessels and other structures such as pathologies and the optic disk. The benefit of this inclusion is studied and presented in Section 4.6. Fig. 8 shows the segmentation obtained using the proposed linear combination process. It can be seen that the aggregation of line responses at different scales has helped to eliminate the background noise while maintaining good segmentation at regions close to the vessels.

## 4. Performance on DRIVE and STARE

The performance of the proposed method was evaluated and compared to most recent methods on two publicly available STARE [17] and DRIVE [6] datasets. STARE dataset consists of 20 retinal images while DRIVE dataset consists of 40 retinal images divided into two sets: the training set and the test set. In DRIVE dataset, for comparison purpose, the performance of the proposed method is measured on 20 test images. In each dataset, the segmentations of the first observer are used as the ground truth for evaluation while the

Table 1

Responses of the basic line detector ( $R_{15}$ ) and generalized line detector ( $R_{15}^3$ ) at different pixel positions presented in Fig. 5. Incorrect responses are highlighted in bold-faced numbers. The basic line detector produces false responses for three cases (d)–(f) while the generalized line detector has shown its improvements when producing expected responses for all cases presented.

Case	(a)	(b)	(c)	(d)	(e)	(f)
$R_{15}$	0.055	0.002	0.028	<b>0.024</b>	<b>0.023</b>	<b>0.013</b>
$R_{15}^3$	0.060	-0.007	0.010	-0.013	-0.031	-0.015
Expected $R$	$R > 0$	$R \approx 0$	$R > 0$	$R \approx 0$	$R \approx 0$	$R \approx 0$

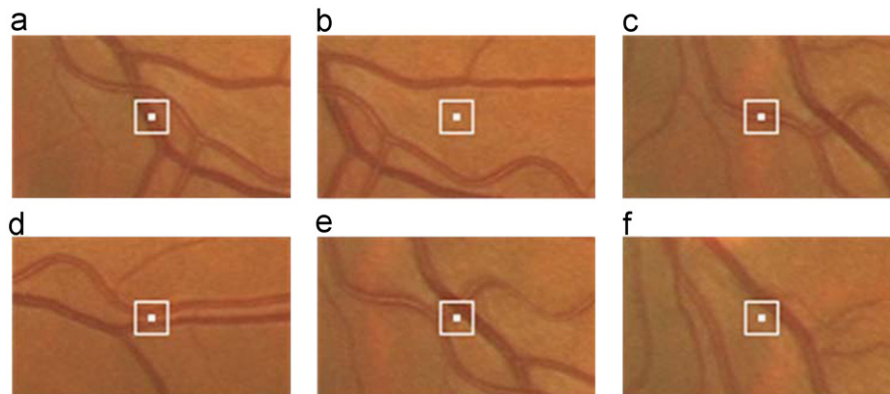
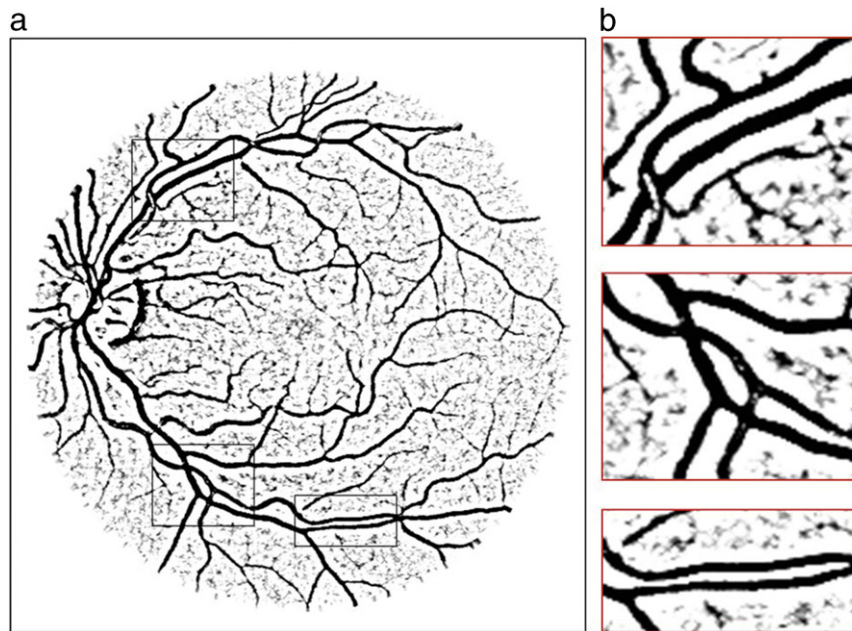
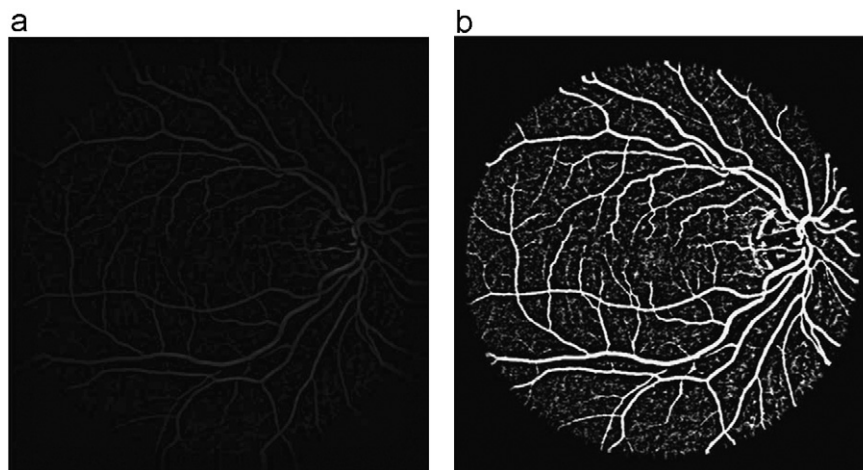


Fig. 5. Different pixel positions on a real image (white dots) and the expected responses  $R$  at: (a) a vessel pixel ( $R > 0$ ); (b) a background pixel ( $R \approx 0$ ); (c) a central reflex pixel ( $R > 0$ ); (d) a background pixel within two close vessels ( $R \approx 0$ ); (e) a background pixel near the crossover point ( $R \approx 0$ ); (f) a background pixel near the strong vessel ( $R \approx 0$ ).



**Fig. 6.** (a) Line strength image of the generalized line detector ( $W = 15, L = 3$ ) on the same retinal image of Fig. 2(a) and (b) segmentation results at some image patches showing its improvements compared to the basic line detector.



**Fig. 7.** Response images of generalized line detector ( $W = 15, L = 3$ ) on a retinal image (a) before and (b) after applying standardization.

performance of the second observer is used as a benchmark for comparison.

#### 4.1. Evaluation measures

In this experiment, two measures, the accuracy (ACC) and local accuracy (Local ACC), are used as main measures for evaluation and comparison. The accuracy has been widely used in this area as the main measure for evaluation and is measured by the ratio of the total number of correctly classified pixels (sum of true positives and true negatives) to the number of pixels in the image field of view (a mask image which defines the field of view is provided for each retinal image). We call this global accuracy since all pixels within the fundus are used for the computation. However, since background pixels often occupy more than 80% of a retinal image, the global accuracy obtained are always high and there is only a small discrimination in accuracy values of different methods. Motivated by this and by the fact that most of the following analysis (i.e., vessel caliber measurement or crossover point abnormality detection) are performed using pixels within a certain distance from the true

vessels, the local accuracy is also used as an additional measure. In this measure, only vessel and background pixels around the true vessels are considered for accuracy measurement. To achieve this, the ground truth image is dilated using morphological dilation operator with a structuring element of size  $S$  and this dilated version is used as the mask for accuracy measurement. The local accuracy of different methods are reported with  $S = 3$ , since at this value an equal number of vessel and background pixels are considered for accuracy computation. In this experiment, paired two sided Wilcoxon sign rank tests are used to check for significant difference.

#### 4.2. Parameter setting

Parameter setting of the proposed method on these datasets is as follows.<sup>1</sup>  $W$  is set to 15 pixels (since vessel width in these images is around 7–8 pixels) and the line responses at 8 scales

<sup>1</sup> The source code and segmentation results of the proposed method can be accessed online at: [http://people.eng.unimelb.edu.au/thivun/projects/retinal\\_segmentation/](http://people.eng.unimelb.edu.au/thivun/projects/retinal_segmentation/)

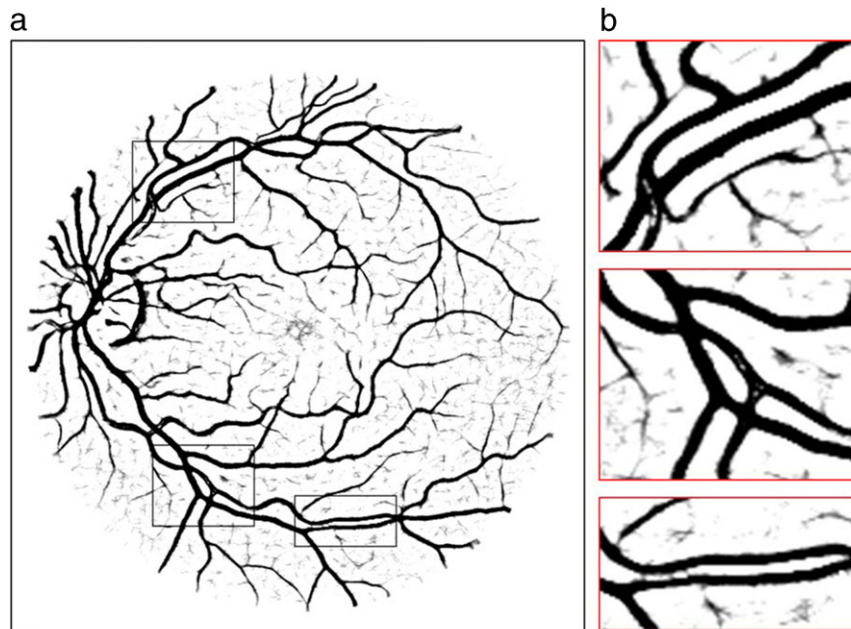


**Fig. 8.** (a) Line strength image obtained after the linear combination process on the same retinal image of Fig. 2(a) and (b) segmentation results at some image patches showing its improvements over the individual line detectors.

(from 1 to 15 with a step of 2) are linearly combined to produce the final segmentation for each image. The segmentation obtained by our method is a soft classification where each value represents the probability of each pixel of belonging to the vessel class. A single threshold is then used to segment the soft classification and produce binary segmentation for each retinal image. In order to choose the threshold value, 20 images in DRIVE training set are used to tune the threshold parameter. The threshold value that produces highest average accuracy on the training set is at  $t=0.56$ . Hence, the same threshold value ( $t=0.56$ ) is used to segment all images in DRIVE test set and STARE dataset.

#### 4.3. Quantitative assessment

Table 2 presents the performance of different methods in terms of accuracy and local accuracy on DRIVE and STARE datasets. All of these values were computed using the segmentation results produced by each method. The segmentations of Staal et al. [6], Niemeijer et al. [22], Jiang et al. [28], Perez et al. (on DRIVE images) [30], Zana et al. [27], Chaudhuri et al. [16] methods are downloaded from DRIVE website.<sup>2</sup> Results of Soares et al.<sup>3</sup> [7], Marin et al.<sup>4</sup> [25], Perez et al.<sup>5</sup> (on STARE images) [30] methods are obtained from their websites. Results of Lupascu et al. [24] method are provided by the authors. Since the segmentation results of Ricci et al. methods are not available for comparison, we implemented the two methods proposed by Ricci et al. [8], the unsupervised method (denoted as 'Ricci-line') and supervised method (denoted as 'Ricci-svm'). To get the binary segmentations returned by Ricci-line method, different thresholds are examined and the one that provides highest average accuracy on each dataset is chosen. However, we cannot achieve the accuracy as presented in that paper (also reported by Lam et al. [32]). Regarding the Ricci-svm method, we implemented it using the conditions described in the paper (i.e. linear SVM with

$C_- = 1$  and  $C_+ = 7$ ) but the average accuracy obtained is much lower than the reported one. Hence, different parameter settings for SVM model were tested and the performance obtained with the optimal setting (nonlinear SVM using RFB kernel with  $C_- = C_+ = 1$  and  $\gamma = 2$ ) is reported in this paper.

The results show that the accuracy of the proposed method is higher than most of unsupervised methods (except Perez et al. and Ricci-line on STARE) with  $p < 0.03$ , and approaches the performance of other supervised methods on both datasets. More importantly, the results show that the local accuracy of our proposed method is higher than all unsupervised and supervised methods ( $p < 0.002$ ) and approaches the performance of the second observer on DRIVE dataset. On STARE dataset, the local accuracy of the proposed method also approaches the performance of the second observer, be comparable to Soares and Perez et al. methods and keep higher than other methods ( $p < 0.0008$ ).

Figs. 9 and 10 show the local accuracy of different methods when the structuring element size  $S$  (the parameter used for local accuracy measurement) increases from 1 to 10 on DRIVE and STARE datasets, respectively. The two graphs show that the local accuracy achieved by our method is higher than those of the other methods at small sizes of  $S$  ( $S$  from 1 to 4) and is comparable to other methods at larger structuring element sizes  $S$ . It should be noted that at small sizes of  $S$ , the errors in the local accuracy measurement mainly comes from the misclassification of vessel pixels to background pixels. Visually, these false negatives are presented in the segmentation result as the presence of central reflex artefacts, vessel disconnection or the missing of small vessels. The superior performance at these small sizes of  $S$  has demonstrated the capability to give accurate segmentation around the vessel regions of the proposed method.

#### 4.4. Qualitative assessment

The improvements of the proposed method over existing methods in terms of local accuracy can also be observed on the segmentation results. To demonstrate this, the segmentation results obtained by our method and those of two supervised

<sup>2</sup> <http://www.isi.uu.nl/Research/Databases/DRIVE/>

<sup>3</sup> <http://retina.iv.fapesp.br>

<sup>4</sup> <http://uhu.es/retinopathy/eng/bd.php>

<sup>5</sup> <http://turing.iimas.unam.mx/elena/Projects/segmenta/DRIVE.html>

methods, Staal et al., Soares et al., and Ricci-line method at some selective regions (regions with the presence of central light reflex and close vessels) are presented in Fig. 11 for comparison. It can be observed that both Staal and Soares et al. methods are ineffective in dealing with central reflex when assigning those pixels at the center of central reflex vessels as background.

**Table 2**  
Performance of different segmentation methods in terms of ACC and local ACC ( $S=3$ ) on DRIVE and STARE datasets.

Method	DRIVE		STARE	
	ACC	Local ACC	ACC	Local ACC
Second observer	0.9473	0.7921	0.9350	0.7706
<i>Supervised methods</i>				
Staal et al. [6]	0.9442	0.7749	–	–
Soares et al. [7]	0.9466	0.7772	0.9480	0.7525
Lupascu et al. [24]	0.9409	0.7604	–	–
Niemeijer et al. [22]	0.9416	0.7562	–	–
Marin et al. [25]	0.9448	0.7710	0.9481	0.7322
Ricci-svm [8]	0.9424	0.7590	0.9496	0.7276
<i>Unsupervised methods</i>				
Jiang et al. [28]	0.9222	0.6915	–	–
Hoover et al. [17]	–	–	0.9240	0.6998
Perez et al. [30]	0.9316	0.7670	0.9196	0.7607
Zana et al. [27]	0.9320	0.7318	–	–
Chaudhuri et al. [16]	0.8884	0.5587	–	–
Ricci-line [8]	0.9329	0.7413	0.9356	0.7285
<b>Proposed method</b>	<b>0.9407</b>	<b>0.7883</b>	<b>0.9324</b>	<b>0.7630</b>

Moreover, Soares and Ricci-line methods tends to merge two close vessels together. On the contrary, the proposed method provides correct vessel response at central reflex pixels while keeping close vessels well separated.

#### 4.5. Execution time

Table 3 presents the execution time of different methods on DRIVE and STARE datasets. On a PC Intel Duo Core 2.4 GHz CPU and 2 GB RAM, it takes 2.5 s to segment a DRIVE or STARE image using our proposed method. The proposed method is efficient since its segmentation time is fast and no training time is needed. Currently, the implementation is in Matlab and no optimization is performed. So, the execution time could be reduced further. In addition, since only linear filtering is involved, the proposed method can be easily extended to work on high resolution retinal images.

#### 4.6. Discussions

Currently, the proposed method works extremely well on healthy retinal images even in the presence of vessel central reflex. However, a drawback of the proposed method is that it tends to produce false vessel detection around the optic disk and pathological regions such as dark and bright lesions. This has lowered the overall accuracy of the proposed method especially on STARE images. This limitation has been demonstrated in Fig. 12.

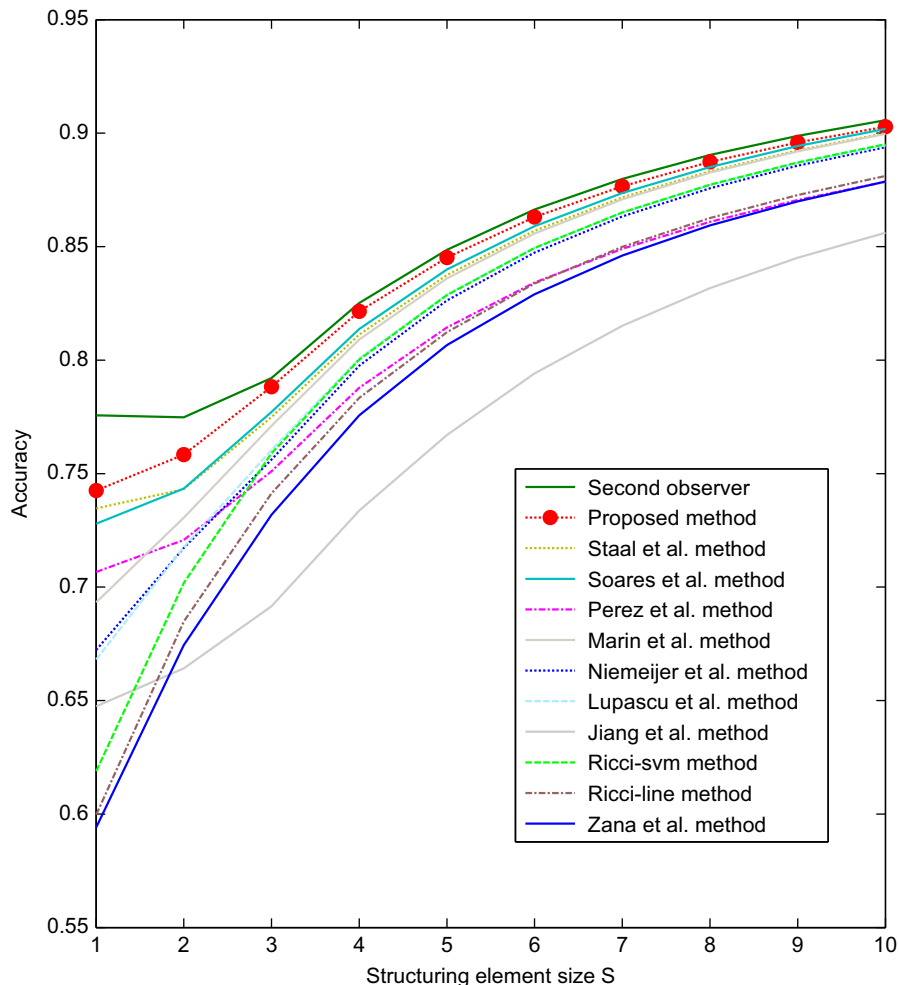


**Fig. 9.** Local ACC of different methods on DRIVE when S increases from 1 to 10.



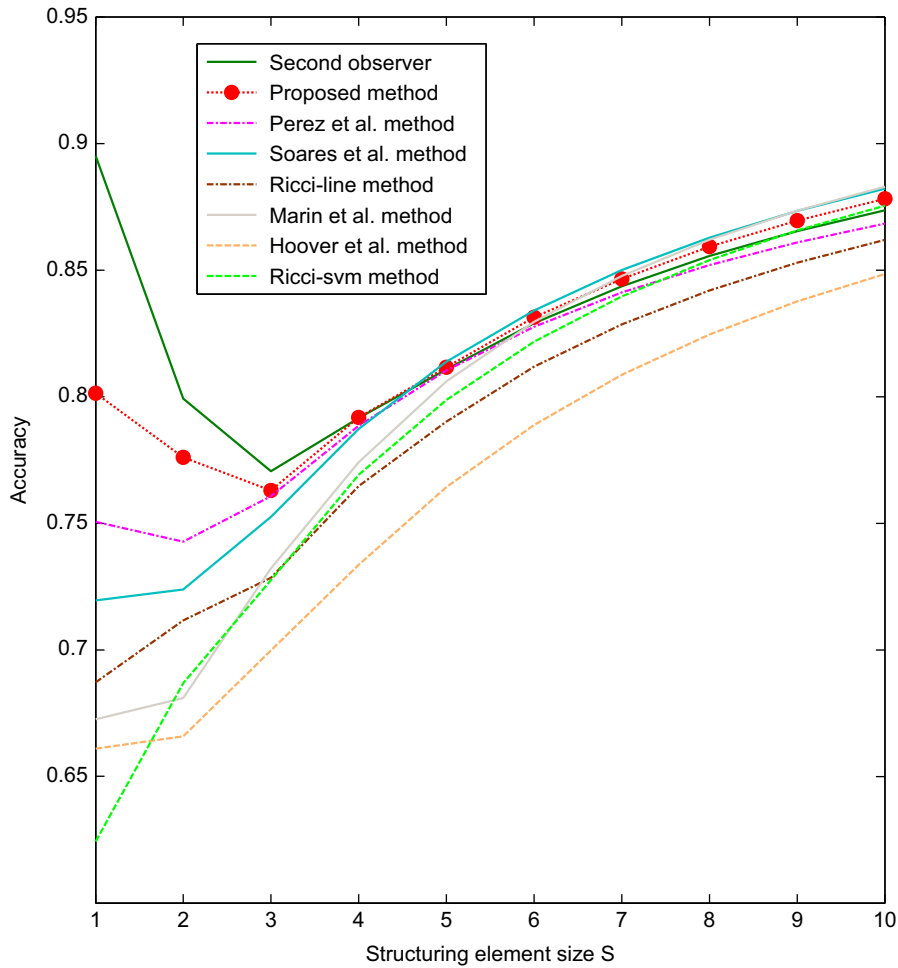


Fig. 10. Local ACC of different methods on STARE when S increases from 1 to 10.

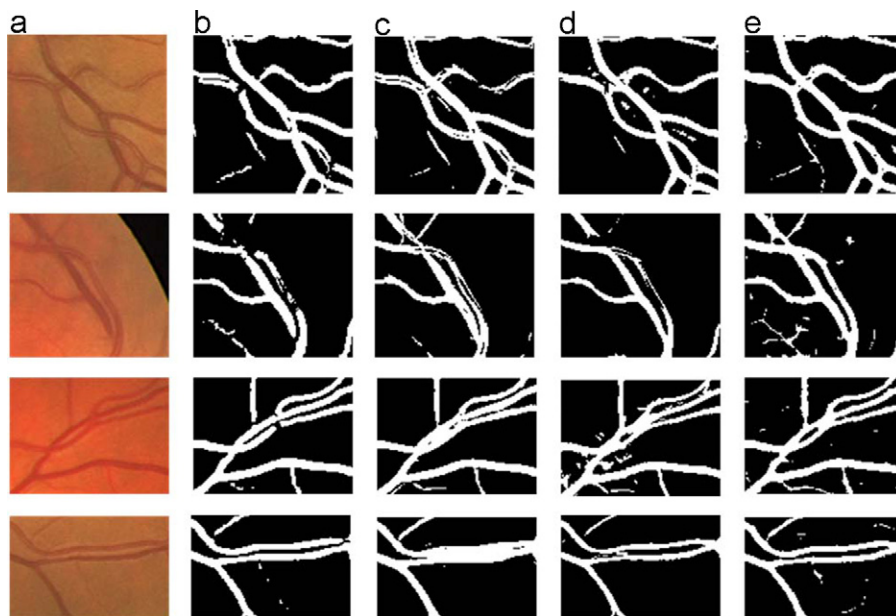


Fig. 11. Segmentation results on some selective regions showing the improvements of the proposed method over existing methods in terms of segmentation quality: (a) original image; segmentations of (b) Staal et al. method; (c) Soares et al. method; (d) Ricci-line method; and (e) proposed method.

To solve this problem, a post-processing step to localize these regions would help to reduce these false positives and improve the performance of the method further.

In addition, to investigate the benefit of the green channel in the combination process described in Section 3.3, we explored the performance achieved by the proposed method when the green

channel is included and excluded from the combination and the results are presented in Table 4. It is shown that the inclusion of the green channel has helped to improve the performance of our

**Table 3**  
Performance of different segmentation methods in terms of execution time on DRIVE and STARE datasets.

Method	Running time
Second observer	7200 s
Staal	900 s
Soares	190 s(9 h for training)
Lupascu	125 s (4 h for training)
Marin	90 s
Ricci-SVM	79 s(20 s for training)
Ricci-line	0.37 s
<b>Proposed method</b>	<b>2.5 s</b>

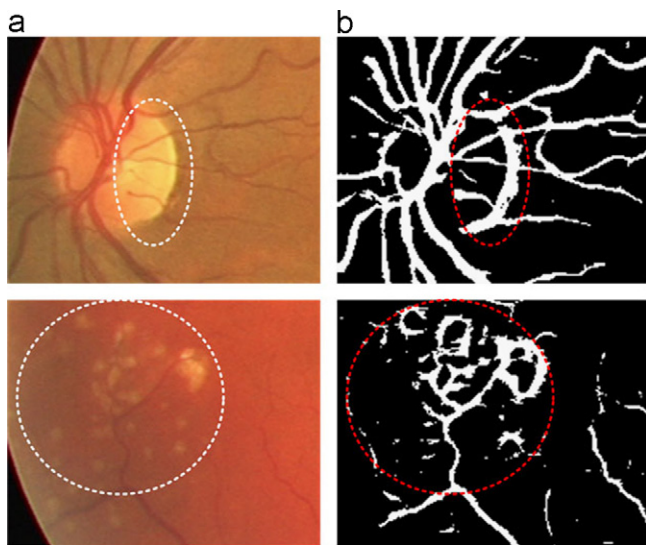


**Fig. 12.** Examples show the limitations of the proposed method: (a) original image; (b) segmented image. Top row: the segmentation shows false vessel detection around the optic disk. Bottom row: the segmentation shows false vessel response at pathological region (i.e., bright lesions).

**Table 4**  
Performance achieved by the proposed method on DRIVE and STARE datasets when the green channel is included in and excluded from the combination process.

Dataset	ACC		Local ACC	
	Included	Excluded	Included	Excluded
DRIVE	0.9407	0.9373	0.7883	0.7860
STARE	0.9324	0.9248	0.7630	0.7554

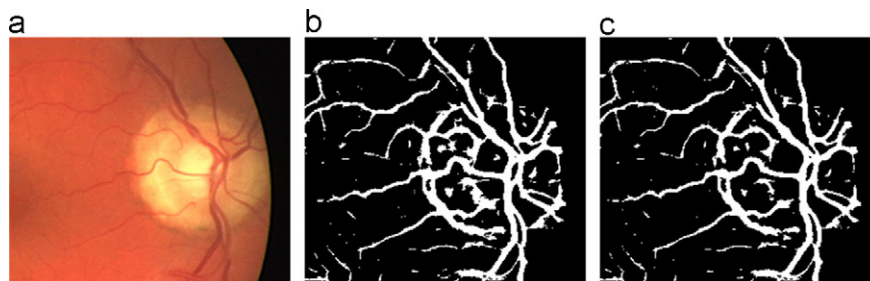


**Fig. 13.** An example shows the effect of including the original green channel into the combination process: (a) a cropped retinal image at the optic disk; the segmentations obtained (b) without and (c) with the inclusion of the original green channel. The inclusion of the green channel has helped to reduced false vessel responses at the optic disk region.

method on both DRIVE and STARE datasets. This improvement comes from the reduction in the number of false positives at the optic disk and pathological regions when the green channel is included into the combination. An example of this improvement is demonstrated in Fig. 13. Hence, the green channel has been included into the combination to improve the segmentation accuracy of our proposed method.

## 5. Performance on REVIEW

In this experiment, we aim at assessing the applicability of the proposed method to provide accurate vessel width measurement on retinal images with the presence of central reflex. This is motivated by the fact that the vessel width is an important factor for disease prediction and it is one of the ultimate goals of retinal image analysis. This experiment was performed on REVIEW dataset [34], a retinal vessel reference dataset which was designed to assess the accuracy and precision of the vessel width measurement algorithms in the presence of pathologies and central light reflex. The vessel width measurements obtained using the segmentations produced by our method are compared against the measurements done by the human observers. Comparison is also made to the results obtained using the segmentations produced by Ricci-line method. The performance of the proposed method was evaluated using two retinal images (CLRIS001 and CLRIS002) in the CLRIS (Central Light Reflex Image Set) set. These two images contain 21 vessel segments (3 in CLRIS001 and 18 in CLRIS002) with 285 profiles manually marked by three independent observers. Fig. 14 shows a retinal image in this set with three vessel segments manually marked by the first observer.

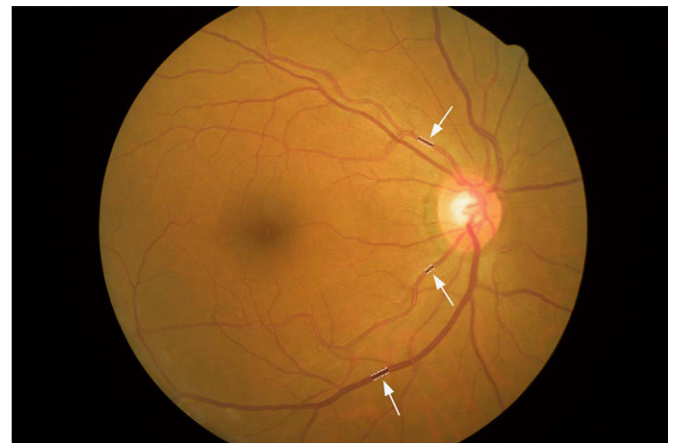


**Fig. 14.** A retinal image in CLRIS set with three vessel segments manually marked by the first observer.



Fig. 15. (a) A portion of CLRS002 image and segmentations obtained by (b) Ricci-line method and (c) our proposed method.

5.1. Parameter setting

Parameter setting for our proposed method on this dataset is as follows.  $W$  is set to 41 pixels (since vessel width in these images is approximately 20 pixels on average) and the line responses at 21 scales (from 1 to 41 with a step of 2) are linearly combined to produce the final segmentation for each image. The same threshold value ( $t=0.56$ ) is used to segment the soft classification and produce the binary segmentation for images in this set. It takes 84 s for our method to segment an image ( $2160 \times 1440$  pixels) in this set. Fig. 15 shows the segmentations obtained by the proposed method and Ricci-line method on a cropped retinal image in this set. It can be observed that in the segmentation produced by the Ricci-line method, there are many false positive pixels at regions between two close vessels. If either one of these two vessels is considered for vessel width measurement, the false positives along these vessels will affect the measurement process and decrease the accuracy of the measurements obtained. The improvements of the result produced by our proposed method over Ricci-line method can be observed in this segmentation result (Fig. 15(c)) as there are no false positives at regions between these two vessels.

From the segmentation obtained by each method, the points along the vessel edge are extracted and fed to a method for automatic vessel width measurement. For comparison, we identify the center points of all profiles which were manually marked by an observer. An automatic method will use the edge image extracted and identify the profile at each center point.

5.2. Vessel width measurement method

This method is designed to identify a pair of edge points representing the width of a vessel at a specific center point. At each center point, all edge points (points in the edge image) that are within a certain mask centered on the center point are located. For each edge point, its mirror point which is on the other edge side and forms a  $180^\circ$  angle with current edge point is determined. To efficiently detect the mirror for all edge points, at each edge point  $E_i$ , the angle  $\alpha_i$  formed by the vector pointing from the center point to the edge point and the vector representing the horizontal line is computed. An edge point  $E_j$  is considered as the mirror point of  $E_i$  if:

$$-\epsilon < |\alpha_i - \alpha_j| - 180 < \epsilon \tag{5}$$

where  $\epsilon$  is a small positive value defining the acceptable difference between the angle formed by two edge points and the difference in the ideal case,  $180^\circ$ . It is set as  $5^\circ$  in our experiment. From the set of pairs of edge points, the pair of edge points with the shortest length is identified as the edge points representing the vessel width (Fig. 16).

Fig. 17(a) shows a portion of image CLRS001 with a vessel segment (with the presence of central reflex) manually marked by the first observer. The average of vessel width along this segment is computed as 14.8 pixels using the profiles manually marked by the expert. Fig. 17(c) shows the vessel profiles along the corresponding segment that were automatically detected using the

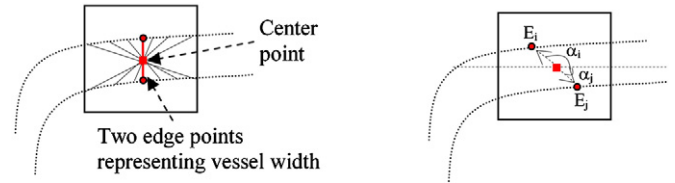


Fig. 16. Method for identifying vessel edge points representing vessel width at a center point.

segmentation produced by our method (Fig. 17(b)). The average of vessel width returned by the automatic method along this segment is computed as 14.82 pixels. This has demonstrated that the proposed segmentation method produces very accurate segmentation along this vessel.

5.3. Results

Table 5 presents the vessel widths (in terms of pixel) on 21 vessel segments of CLRS001 and CLRS002 images measured by the three observers (Obs. 1, Obs. 2 and Obs. 3), Ricci-line and the proposed method. It is worth noting that among the three observers, the first observer (Obs. 1) is an ophthalmic specialist, the second (Obs. 2) is a specialist optometrist and the third (Obs. 3) is a trained grader.<sup>6</sup> Hence, we use the mean values of the measurements provided by the two specialists (Obs. 1 and Obs. 2) as the ground truth measurements while the measurements of the trained grader (Obs. 3) are evaluated for comparison purpose. To assess the performance of each measurement method, the mean absolute error is used:

$$MAE(A,M) = \frac{1}{N} \sum_{i=1}^N |A_i - M_i| \tag{6}$$

where  $N$  is the number of vessel segments considered,  $A_i$  is the measurement produced by method  $A$  and  $M_i$  is the ground truth measurement, respectively, at the  $i$ -th segment. The performances of different methods in terms of mean absolute error are presented in the last row of Table 5.

The results show that the measurements produced by the proposed method are more accurate than the Ricci-line method. This is reflected by the fact that the mean absolute error of the proposed method is of 1.19 pixels while this error of Ricci-line method is 2.08 pixels. In addition, it should be noted that the error of the proposed method is even lower than the error of the trained grader (Obs. 3). This has demonstrated the fact that the proposed method produces highly accurate segmentation which can be used for automatic vessel width measurement process.

6. Conclusions

In this paper, we proposed a novel retinal blood vessel segmentation method which is based on the linear combination

<sup>6</sup> <http://reviewdb.lincoln.ac.uk/REVIEWDB/REVIEWDB.aspx>



**Fig. 17.** Results of vessel width measurement on a vessel segment: (a) a cropped retinal image with vessel profiles representing the vessel width manually marked by an observer; (b) segmentation produce by the proposed method; (c) the vessel profiles automatically marked using the segmentation produced by the proposed method.

**Table 5**  
Vessel width measurements and mean absolute error (MAE) of different methods on 21 vessel segments of CLRIS001 and CLRIS002 images.

Segment No.	Mean of vessel width				
	Obs. 1	Obs. 2	Obs. 3	Ricci-line	Proposed method
<b>CLRIS001</b>					
1	14.80	15.98	18.12	15.69	15.09
2	15.15	16.34	16.88	16.33	15.68
3	17.63	19.87	19.51	18.70	18.86
<b>CLRIS002</b>					
1	11.41	10.46	12.88	13.60	13.46
2	20.15	20.28	21.86	19.80	19.95
3	20.68	20.53	21.23	20.01	20.14
4	19.35	19.31	20.69	18.77	19.24
5	15.95	16.17	17.49	15.35	15.84
6	10.82	10.36	12.44	13.43	13.42
7	11.14	10.70	13.82	15.28	15.11
8	11.36	10.31	13.33	13.04	12.98
9	13.36	13.35	14.30	14.22	13.80
10	10.01	9.63	10.50	7.27	8.93
11	11.45	14.12	14.14	14.56	14.05
12	12.54	14.29	13.33	15.86	15.61
13	15.65	16.10	17.07	17.32	16.49
14	10.87	12.09	12.07	11.91	12.19
15	8.07	7.89	8.62	10.25	9.94
16	12.88	13.61	14.20	25.68	12.72
17	7.74	7.17	8.13	9.53	9.72
18	7.44	7.85	8.07	5.44	6.74
<b>MAE</b>	<b>-</b>	<b>-</b>	<b>1.26</b>	<b>2.08</b>	<b>1.19</b>

of line detectors at varying scales. Experimental results have shown that the proposed method produces comparable accuracy (0.9407 for DRIVE and 0.9324 for STARE) while providing high local accuracy (0.7883 for DRIVE and 0.7630 for STARE, which is higher than any other methods) on DRIVE and STARE datasets. These results have demonstrated the high segmentation accuracy of the proposed method especially at regions around the vessels, where it is most important. This is also observed in the segmentation results shown in some examples in this article. The high segmentation accuracy of the proposed method is also confirmed by the accurate vessel width measurements produced by the proposed method on 21 segments of two retinal images in REVIEW dataset. The results show that the vessel width measurements obtained using the segmentations of the proposed method are highly correlated to the measurements provided by the experts with a mean absolute error of 1.19 pixels (while this error of the trained grader is 1.26 pixels). With these significant improvements, we conclude that our method will be very effective for vascular network mapping and vessel caliber measurement. In addition, compared to other approaches, our method is efficient with fast segmentation time (2.5 s per image) and can be easily scaled to deal with high resolution retinal images. Moreover, as being an unsupervised method, the proposed method is helpful when manual segmentations are not available for training purpose. In the future, we plan to apply our method to extract and

analyze the vascular network to detect arteriovenous nicking for cardiovascular disease prediction.

## References

- [1] B. Wasan, A. Cerutti, S. Ford, R. Marsh, Vascular network changes in the retina with age and hypertension, *Journal of Hypertension* 13 (12) (1995) 1724–1728.
- [2] T.Y. Wong, R. McIntosh, Hypertensive retinopathy signs as risk indicators of cardiovascular morbidity and mortality, *British Medical Bulletin* 73 (1) (2005) 57–70.
- [3] E.J. Sussman, W.G. Tsiaras, K.A. Soper, Diagnosis of diabetic eye disease, *JAMA: The Journal of the American Medical Association* 247 (23) (1982) 3231–3234.
- [4] T.Y. Wong, R. Klein, D.J. Couper, L.S. Cooper, E. Shahar, L.D. Hubbard, M.R. Wofford, A.R. Sharrett, Retinal microvascular abnormalities and incident stroke: the atherosclerosis risk in communities study, *The Lancet* 358 (9288) (2001) 1134–1140.
- [5] T.Y. Wong, R. Klein, A.R. Sharrett, B.B. Duncan, D.J. Couper, B.E.K. Klein, L.D. Hubbard, F.J. Nieto, Retinal arteriolar diameter and risk for hypertension, *Annals of Internal Medicine* 140 (4) (2004) 248–255.
- [6] J. Staal, M.D. Abramoff, M. Niemeijer, M.A. Viergever, B. van Ginneken, Ridge-based vessel segmentation in color images of the retina, *IEEE Transactions on Medical Imaging* 23 (4) (2004) 501–509.
- [7] J.V.B. Soares, J.J.G. Leandro, R.M. Cesar, H.F. Jelinek, M.J. Cree, Retinal vessel segmentation using the 2-d gabor wavelet and supervised classification, *IEEE Transactions on Medical Imaging* 25 (9) (2006) 1214–1222.
- [8] E. Ricci, R. Perfetti, Retinal blood vessel segmentation using line operators and support vector classification, *IEEE Transactions on Medical Imaging* 26 (10) (2007) 1357–1365.
- [9] M. Fraz, P. Remagnino, A. Hoppe, B. Uyyayanonvara, A. Rudnicka, C. Owen, S. Barman, Blood vessel segmentation methodologies in retinal images—a survey, *Computer Methods and Programs in Biomedicine*.
- [10] I. Liu, Y. Sun, Recursive tracking of vascular networks in angiograms based on the detection-deletion scheme, *IEEE Transactions on Medical Imaging* 12 (2) (1993) 334–341.
- [11] L. Zhou, M.S. Rzeszotarski, L.J. Singerman, J.M. Chokreff, The detection and quantification of retinopathy using digital angiograms, *IEEE Transactions on Medical Imaging* 13 (4) (1994) 619–626.
- [12] O. Chutatape, L. Zheng, S. Krishnan, Retinal blood vessel detection and tracking by matched gaussian and kalman filters, in: *Engineering in Medicine and Biology Society, 1998. Proceedings of the 20th Annual International Conference of the IEEE, vol. 6, IEEE, 1998, pp. 3144–3149.*
- [13] Y.A. Toliás, S.M. Panas, A fuzzy vessel tracking algorithm for retinal images based on fuzzy clustering, *IEEE Transactions on Medical Imaging* 17 (2) (1998) 263–273.
- [14] A. Can, H. Shen, J.N. Turner, H.L. Tanenbaum, B. Roysam, Rapid automated tracing and feature extraction from retinal fundus images using direct exploratory algorithms, *IEEE Transactions on Information Technology in Biomedicine* 3 (2) (1999) 125–138.
- [15] Y. Yin, M. Adel, S. Bourenane, Retinal vessel segmentation using a probabilistic tracking method, *Pattern Recognition* 45 (2012) 1235–1244.
- [16] S. Chaudhuri, S. Chatterjee, N. Katz, M. Nelson, M. Goldbaum, Detection of blood vessels in retinal images using two-dimensional matched filters, *IEEE Transactions on Medical Imaging* 8 (3) (1989) 263–269.
- [17] A. Hoover, V. Kouznetsova, M. Goldbaum, Locating blood vessels in retinal images by piecewise threshold probing of a matched filter response, *IEEE Transactions on Medical Imaging* 19 (3) (2000) 203–210.
- [18] M. Al-Rawi, M. Qutaishat, M. Arrar, An improved matched filter for blood vessel detection of digital retinal images, *Computers in Biology and Medicine* 37 (2) (2007) 262–267.
- [19] L. Zhang, Q. Li, J. You, D. Zhang, A modified matched filter with double-sided thresholding for screening proliferative diabetic retinopathy, *IEEE Transactions on Information Technology in Biomedicine* 13 (4) (2009) 528–534.
- [20] B. Zhang, L. Zhang, F. Karray, Retinal vessel extraction by matched filter with first-order derivative of gaussian, *Computers in Biology and Medicine* 40 (4) (2010) 438–445.
- [21] C. Sinthanayothin, J.F. Boyce, H.L. Cook, T.H. Williamson, Automated localisation of the optic disc, fovea, and retinal blood vessels from digital colour fundus images, *British Journal of Ophthalmology* 83 (8) (1999) 902.

- [22] M. Niemeijer, J. Staal, B. van Ginneken, M. Loog, M. D. Abramoff, Comparative study of retinal vessel segmentation methods on a new publicly available database, in: *Proceedings of SPIE*, vol. 5370, 2004, pp. 648–656.
- [23] M. Sofka, C.V. Stewart, Retinal vessel centerline extraction using multiscale matched filters, confidence and edge measures, *IEEE Transactions on Medical Imaging* 25 (12) (2006) 1531–1546.
- [24] C.A. Lupascu, D. Tegolo, E. Trucco, Fabc: retinal vessel segmentation using adaboost, *IEEE Transactions on Information Technology in Biomedicine* 14 (5) (2010) 1267–1274.
- [25] D. Marin, A. Aquino, M.E. Gegúndez-Arias, J.M. Bravo, A new supervised method for blood vessel segmentation in retinal images by using gray-level and moment invariants-based features, *IEEE Transactions on Medical Imaging* 30 (1) (2011) 146–158.
- [26] X. You, Q. Peng, Y. Yuan, Y. Cheung, J. Lei, Segmentation of retinal blood vessels using the radial projection and semi-supervised approach, *Pattern Recognition* 44 (2011) 2314–2324.
- [27] F. Zana, J.C. Klein, Segmentation of vessel-like patterns using mathematical morphology and curvature evaluation, *IEEE Transactions on Image Processing* 10 (7) (2001) 1010–1019.
- [28] X. Jiang, D. Mojon, Adaptive local thresholding by verification-based multi-threshold probing with application to vessel detection in retinal images, *IEEE Transactions on Pattern Analysis and Machine Intelligence* (2003) 131–137.
- [29] K. Vermeer, F. Vos, H. Lemij, A. Vossepoel, A model based method for retinal blood vessel detection, *Computers in Biology and Medicine* 34 (3) (2004) 209–219.
- [30] M.E. Martinez-Perez, A.D. Hughes, S.A. Thom, A.A. Bharath, K.H. Parker, Segmentation of blood vessels from red-free and fluorescein retinal images, *Medical Image Analysis* 11 (1) (2007) 47–61.
- [31] B.S.Y. Lam, H. Yan, A novel vessel segmentation algorithm for pathological retina images based on the divergence of vector fields, *IEEE Transactions on Medical Imaging* 27 (2) (2008) 237–246.
- [32] B.S.Y. Lam, Y. Gao, A.W.C. Liew, General retinal vessel segmentation using regularization-based multiconcavity modeling, *IEEE Transactions on Medical Imaging* 29 (7) (2010) 1369–1381.
- [33] M. Vlachos, E. Dermatas, Multi-scale retinal vessel segmentation using line tracking, *Computerized Medical Imaging and Graphics* 34 (3) (2010) 213–227.
- [34] B. Al-Diri, A. Hunter, D. Steel, M. Habib, T. Hudaib, S. Berry, Review-a reference data set for retinal vessel profiles, in: *Engineering in Medicine and Biology Society, 2008. EMBS 2008, 30th Annual International Conference of the IEEE, IEEE, 2008*, pp. 2262–2265.

**Uyen T.V. Nguyen** received the BSc degree from Ho Chi Minh University of Technology, Vietnam in 2006 and the Master degree from KyungHee University, Korea in 2008. She is currently a PhD student at Department of Computer Science and Software Engineering, the University of Melbourne, Australia. Her research interest includes Clustering, Image Processing, Medical Imaging, and Computer Vision.

**Dr. Alauddin Bhuiyan** received the BE degree from Shahjalal University of Science and Technology, Bangladesh and PhD degree from the University of Melbourne, Australia. He is currently working as a research fellow at Commonwealth Scientific and Industry Research Organization (CSIRO), ICT Perth, Australia. Before joining at CSIRO he worked as a research fellow at Centre for Eye Research Australia and Department of Computer Science and Software Engineering at the University of Melbourne. His research interests include Medical Imaging, Computer Vision, Pattern Recognition and Artificial Intelligence. He is a member of IEEE and IAPR.

**Dr. Laurence A.F. Park** received the BE (Hons.) and BSc degrees from the University of Melbourne, Australia, in 2000, and the PhD degree from the University of Melbourne in 2004. He joined the Computer Science Department at the University of Melbourne as a research fellow in 2004, and was promoted to a senior research fellow in 2008. He joined the School of Computing and Mathematics at the University of Western Sydney as a lecturer in computational mathematics and statistics in 2009, where he is currently investigating methods of large-scale data mining and machine learning. During this time, he has been made an honorary senior fellow of the University of Melbourne.

**Prof. Ramamohanarao (Rao) Kotagiri** received PhD from Monash University. He was awarded the Alexander von Humboldt Fellowship in 1983. He has been at the University Melbourne since 1980 and was appointed as a professor in computer science in 1989. Rao held several senior positions including Head of Computer Science and Software Engineering, Head of the School of Electrical Engineering and Computer Science at the University of Melbourne and Research Director for the Cooperative Research Centre for Intelligent Decision Systems. He served on the Editorial Boards of the *Computer Journal*. At present he is on the Editorial Boards for *Universal Computer Science*, and *Data Mining, IEETKDE and VLDB (Very Large Data Bases) Journal*. He was the program Co-Chair for VLDB, PAKDD, DASFAA and DOOD conferences. He is a steering committee member of IEEE ICDM, PAKDD and DASFAA. He received distinguished contribution award for Data Mining. Rao is a Fellow of the Institute of Engineers Australia, a Fellow of Australian Academy Technological Sciences and Engineering and a Fellow of Australian Academy of Science. He was awarded Distinguished Contribution Award in 2009 by the Computing Research and Education Association of Australasia.